Characterizing Solute Segregation and Grain Boundary Energy in a Binary Alloy Phase Field Crystal Model

Jonathan Stolle*
Department of Physics and Astronomy, McMaster University, 1280 Main Street West, Hamilton, Ontario L8S-4L7

Nikolas Provatas†
Department of Physics, McGill University, 3600 rue University, Montreal, Quebec H3A-2T8

(Dated: today)

This paper studies solute segregation and its relationship to grain boundary energy in binary alloys. Grain boundaries are simulated using a binary alloy phase field crystal model that incorporates atomic elasto-plastic effects on diffusional time scales. Grain boundary energy versus misorientation data is semi-empirically fit to Read-Shockely theory in order to characterize its dependence on the average alloy concentration and undercooling below the solidus. The Gibbs Adsorption Theorem is then used to derive a semi-analytic function describing solute segregation to grain boundaries. Our results are in good agreement with direct simulations of the binary alloy PFC model. We also investigate how size mismatch between different species and their interaction strength affects segregation to the grain boundary. We interpret the implications of our simulations on the material properties related to interface segregation.

I. INTRODUCTION

Microstructure in metals is important for determining many of their properties (e.g., mechanical, thermodynamic, electrical). The various defects associated with microstructure formation (e.g., grain boundaries, dislocations, vacancies) contribute to an excess of free energy of a system. As a material evolves towards equilibrium, its microstructure changes and along with it the material's properties. Grain boundaries are among the most important defects in metals. Their energy, composition, and distribution directly affect the flow of dislocations and influence the thermodynamics of second phase and precipitate formation. Being able to determine grain boundary properties is therefore crucial to be able to properly model the myriad multi-scale properties linked to grain boundaries in solidification and solid state transformations.

In an alloy, segregation of solute atoms can alter grain boundary energy [1–3]. The effect of segregation can also manifest itself in other ways. Two other properties strongly affected by solute segregation are solute drag [2, 4, 5] and grain boundary wetting [2, 6–8]. In the former case, the grain boundary energy is reduced by solute segregation, thus reducing the driving force to reduce surface area (excess free energy) of a grain boundary. In the latter case, solute segregation can dramatically affect the thermodynamics of grain boundary formation; not only can segregation alter at what undercooling grain boundary wetting occurs, but it can allow for different grain boundary states (e.g., grain boundaries widths) [7].

There have been a number of experimental studies of grain boundary energy involving pure materials [9–11] and alloys [1, 11]. Many studies have focused on characterizion of solute segregation and distribution [2, 3] as solute segregation typically has an important effect on grain boundary energy as demonstrated in [1, 12, 13]. For pure materials and dilute alloys, many of these studies have found that the grain boundary energy is well-fit by the well-known Read-Shockley Law when neighbouring grains are misoriented by small angles [9, 11]. It is also possible to adjust the parameters of the Read-Shockley equation to fit a larger range of misorientation angles [9–11].

A number of theoretical approaches have been considered to determine grain boundary energy in metals. The most prevalent, for both pure materials and alloyed metals, are the analytic analytic and semi-analytic dislocation models of Read and Shockley [11, 14] and Van der Merwe [2], and models employing simple thermodynamic considerations of an interface [2, 12]. Various computational approaches have also been employed to determine grain boundary energy in pure metals, including Monte Carlo simulations [15] and lattice statistics [16]. Some computational approaches have also been used to model solutal effects in grain boundaries. These include monte carlo methods [3], molecular dynamics [3, 13] and phase field simulations [7].

Among the continuum theories available to model solidification and solid state transformations, the phase field crystal (PFC) method has recently emerged as a promising method to access the time scales and efficiency of traditional phase field approaches while self-consistently incorporating many salient features of atomic-scale elasto-plasticity inherited form its connections to fundamental microscopic theories [17, 18]. Perhaps the most important impact of the phase field crystal

* stolle@mcmaster.ca
† provata@mcmaster.ca; provata@mcmaster.ca

approach will be its ability to bridge the divide that exists between microscopic models and traditional phase field models [19]. For example, through the application of coarse graining theories, several researches have used PFC theories to compute the magnitude and and orientational dependence of crystal-melt surface tension in pure materials [20, 21] and alloys [22]. PFC simulations of grain boundaries of pure materials have also convincingly elucidated the Read Shockley behaviour for grain boundary energy versus misorientation [23, 24] and details of pre-melting in grain boundaries [24, 25].

In this work, we will use a recent phase field crystal model of binary alloys [17] to study the mesoscale behaviour of how alloying and undercooling affect solute segregation and grain boundary energy in alloys. Numerical simulations in conjunction with an analysis using a a single-mode decomposition of the crystal density field will be exploited to develop an expression for grain boundary segregation by exploiting a modification to the Read-Shockley equation that incorporates the effect of impurity concentration and temperature. We also consider the effects of lattice mismatch on segregation to the grain boundary and the Cottrell atmosphere around a dislocation core.

II. PHASE FIELD CRYSTAL MODEL OF A BINARY ALLOY

The phase field crystal (PFC) model of alloys used in this work is derived in detail in Ref. [17]. The resultant PFC free energy is expressed in terms of a temporally coarse-grained normalized crystal density field and a relative density difference that is analogous to a solute concentration field. In particular, the normalized total density is given by $n = (\rho - \rho_l)/\rho_l$ and the normalized concentration by $\psi = (\rho_1 - \rho_2)/\rho_l$, where the total density ρ is the sum of the density of each species, $\rho = \rho_1 + \rho_2$, and ρ_l is the density of a reference liquid state. The Helmholtz free energy functional expressed in these variables is given by

$$F = \int_V \Big\{ (B_0^L + B_2^L\psi^2)\frac{n^2}{2} + B^X n(2\nabla^2 + \nabla^4)\frac{n}{2} - t\frac{n^3}{3} + v\frac{n^4}{4} + w\frac{\psi^2}{2} + u\frac{\psi^4}{4} + K\frac{|\nabla\psi|^2}{2} + \eta B^X n\psi(\nabla^2 + \nabla^4)n\, d^3\vec{r}\Big\} \quad (1)$$

where B_0^L is the isothermal compressibility of the liquid at $\psi = 0$, B_2^L determines how the isothermal compressibility of the liquid changes with ψ, B^X is related to elastic constants in the solid, and t, v, u are determined by the low order terms of a local expansion of the classical density functional theory description of the material, w is related to the various atomic bond energies, and K is related to w and the lattice spacing [17]. The difference $B_0^L - B^X$ plays the role of normalized temperature variable. All lengths are scaled such that the lattice constant is $a = 4\pi/\sqrt{3}$ when the lattice mismatch parameter $\eta = 0$. The lattice spacing changes with concentration according to the parameter $\eta = (1/a)\,\partial a/\partial\psi$.

Assuming conserved dissipative dynamics for both fields, the evolution equations are:

$$\frac{\partial n}{\partial t} = \nabla^2\left(\frac{\delta F}{\delta n}\right) = \nabla^2\mu_n \quad (2)$$

$$\frac{\partial \psi}{\partial t} = \nabla^2\left(\frac{\delta F}{\delta \psi}\right) = \nabla^2\mu_\psi \quad (3)$$

In Eqs. 2 and 3, the atomic mobilities have been absorbed in the time variable and a noise term reflecting the effect of thermal fluctuations on the evolution of the system has been neglected. The chemical potentials corresponding to each conserved field are given by μ_n=$\delta F/\delta n$ and μ_ψ=$\delta F/\delta\psi$.

Equations 1-3 can be represented on mesoscales by a set of complex order parameter equations, the coefficients of which are directly linked to those of the above PFC model, which is, in turn, linked to a simplified classical density functional theory of freezing. The complex order parameter representation of Eqs. 1-3 has also been shown to reduce to the form of a traditional scalar phase field model with coupled strain effects [19]. To the accuracy of a single-mode approximation, such an analysis thus yields a microscopic connection between continuum elastic effects and solute concentration and temperature.

III. THERMODYNAMICS OF GRAIN BOUNDARIES

To investigate the thermodynamics of segregation behaviour at a grain boundary in a binary alloy, we need to consider grain boundary energy. Grain boundary energy in pure materials can be determined by a number of different methods. For grain boundaries with a small misorientation angle, Read and Shockley derived the relation now named after them,

$$\gamma_{gb} = E_0\theta(A - \ln(\theta)), \quad (4)$$

by considering the grain boundary as an array of dislocations, where the dislocation cores do not overlap. For a 2D crystal, the constants in Eq. 4 are $E_0 = Y_2 b/(8\pi\alpha)$, where Y_2 is the 2D elastic modulus, $\alpha = \sqrt{3}/2$ is a correction factor for hexagonal, as opposed to square, geometry, $b \approx a$ is the Burger's vector of the dislocation, and $A = 1 + \ln(a/r_0) - \ln(2\pi) \approx 1.5 - \ln(2\pi)$, which is related to the core energy by the core radius, r_0 [23, 24]. For high angles, some theoretical approaches consider the forces between atoms in a fixed geometry [2, 16], while others treat the high angle grain boundary as an amphorous phase sandwiched between 2 bulk phases [1].

However, as already noted in [1, 9, 10], the parameters in Eq. 4 can be chosen to give a reasonable fit between for the relation between grain boundary energy and misorientation for much larger angles than those considered in the original problem.

It is reasonable to assume that the form of Eq. 4 will remain valid for binary alloys, with the coefficients E_0 and A modified by the presence of segregated solute, as well as by the degree of undercooling. This hypothesis is consistent with phase field and phase field crystal simulations of a pure material Ref. [24, 26], which used Eq. 4 to model grain boundary energy in pure materials at different undercoolings by fitting the core energy (i.e. parameter A) to temperature.

With the presence of a grain boundary (or any other defect), solute may preferentially segregate to the grain boundary. In deriving this modification in the next sections, we will be guided by the Gibbs' adsorption theorem, which relates the degree of solute segregation to the grain boundary energy and chemical potential of the system according to

$$\left(\frac{\partial \gamma_{gb}}{\partial \mu_x}\right)_{T,p} = -\Gamma_x^{ex} \tag{5}$$

where μ_x is the chemical potential of species x in the binary alloy ($x = 1, 2$) and $\Gamma_x^{ex} = N_x^{ex}/A$, where N_x^{ex} is the excess number of atoms of species x in a unit area A of the grain boundary (unit length in 2D) [2]. It is noted that Eq. 5 can be also be written in terms of the chemical potential difference, $\mu_\psi = \mu_1 - \mu_2$, if Γ_x^{ex} is replaced by Γ_ψ^{ex}, the excess particle difference at the grain boundary.

IV. NUMERICAL RESULTS

A. PFC Simulations

We simulate Eqs. 2 and 3 with the Fourier method outlined in Elder and Grant [23] and Mellenthin et al [24]. Our computations are performed on a 1024x2048 grid with periodic boundary conditions. The grid spacing is $\Delta x = \pi/4\sqrt{(1-2\eta\psi)/(1-4\eta\psi)}$ and the time step is $\Delta t = 1.0$. In this work, the average normalized alloy concentations studied are ψ_0=0,-0.05, 0.1, -0.15, and -0.2 (-0.2 is only considered for the large angle fits). The average normalized density in the PFC model is set to $n_0 = 0$. Bicrystal grain boundaries are formed in alloys whose phase behaviour can be described by a spinodal phase diagram, i.e. $w = 0.088$, except for some instances when $\psi_0 = -0.2$, for which $w = 0.008$ [27]. For each concentration studied, the parameter B_0^L is chosen such that the undercooling is sufficient for grain boundaries to close (that is, the disjoining pressure does not keep the grain boundaries from closing as it could at too small undercooling [7, 24]). The exact value for B_0^L depends on the concentration, however, the undercooling typically varies from -0.02 to -0.06. The other parameters used in Eqs. 2 and 3 are $B_2^L = -1.8$, $B^X = 1$, $t = 0.6$, $v = 1$, $u = 4$, and $K = 4$. Note that $\eta = 0$ except where otherwise indicated.

The basic initial condition for simulating a grain boundary begins with two large grains with a small liquid gap of roughly 10 grid points in between them. For the least deep temperature (B_0^L) quenches, at a given average concentration ψ_0, the temperature parameters is dropped and a grain boundary forms. Quenches to the lowest values of B_0^L are done in multiple steps, quenching first to higher, intermediate temperature, before lowering B_0^L to the final desired value. The crystals are oriented $\theta/2$ and $-\theta/2$ from the 0° crystal reference, respectively. Once a simulation is started the grains quickly form a bicrystal with misorientation, θ. For angles below 4°, the translational offset between the grains, which varies for each orientation, needs to be chosen carefully to allow for dislocations to form as opposed to the crystals rotating and forming one crystal. The grain boundary normal is in the x-direction. The angles chosen were: 1.55°, 2.07°, 2.58°, 3.10°, 4.14°, 5.17°, 6.20°, 8.23°, 10.3°, 12.5°, 15°, 17.5°, 20°, 22.5°, 25°, 27.5°, 30°, 32.5°, 35°, 40°. The small angles are chosen such that an integral number of evenly-spaced dislocations fit within the numerical domain, so that the results can be compared accurately to Eq. 4. Due to periodic boundary conditions, two grain boundaries form. The initial spacing between the two grain boundaries is 512 grid points, which is chosen such that interaction between two grain boundaries is negligible (except at possibly 1.55°). Examples of a low angle and a high angle grain boundaries are shown in Fig. 1.

Grain boundary simulations at each B_0^L were typically run for 100000 time steps. Equilibration of a grain boundary is determined by the standard deviation of the chemical potential, σ_{μ_x}, and its magnitude relative to the mean of the chemical potential, μ_x, where x is ψ or n. If either σ_{μ_c} or σ_{μ_n} is much greater than 10^{-5} or σ_{μ_c}/μ_c or σ_{μ_n}/μ_n is greater than 10^{-2}, simulations are run longer, until the above criteria are met.

B. Calculation of Grain Boundary Energy

Grain boundary energy is given by the excess grand potential per unit area (or length in 2D),

$$\begin{aligned} L_y \gamma_{gb} = L_y w_{gb} \left(f_{gb} - \mu_\psi \psi_{gb} - \mu_n n_{gb}\right. \\ \left. - \left(f_s - \mu_\psi \psi_s - \mu_n n_s\right)\right) \end{aligned} \tag{6}$$

where L_y is the length of the grain boundary, w_{gb} is the width of a region encompassing the grain boundary, f_{gb} is the free energy density of the entire domain (including the grain boundary), f_s is the free energy density of the bulk solid, ψ_{gb} and ψ_s are the average normalized

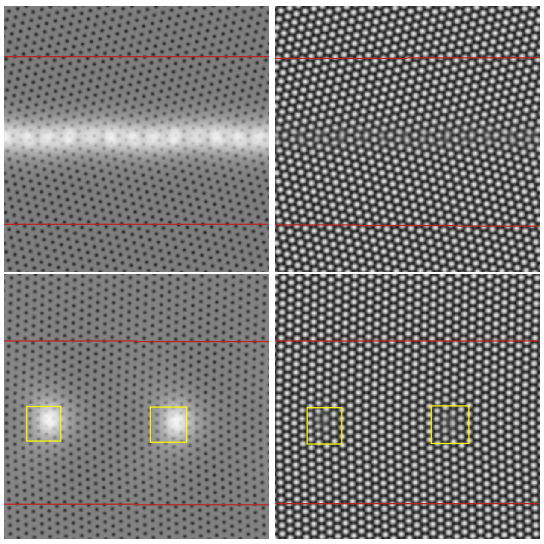

FIG. 1. Images of concentration *(left frames)* and density fields *(right frames)* around low angle *(bottom frames)* and high angle *(top frames)* grain boundaries. The control area enclosing the grain boundary lies between the two red lines. The dislocations in the low angle grain boundary are shown with yellow squares. Note that the x-direction in simulations is the vertical direction in the figures.

concentrations in the grain boundary region and in the bulk solid, respectively, while n_{gb} and n_s are the average normalized atomic densities in the grain boundary region and in the solid, respectively. ψ_{gb} and ψ_s and the analogous normalized density quantities (obtained by substituting ψ with n) are calculated as follows:

$$\psi_{gb} = \frac{1}{L_y w_{gb}} \int_0^{L_y} \int_{x_{gb}-w_{gb}/2}^{x_{gb}+w_{gb}/2} \psi dx dy$$
$$\psi_s = \frac{0.5 L_x \psi_0 - w \psi_{gb}}{0.5 L_x - w_{gb}}$$

Given that the ψ_s and n_s do not differ substantially from the average values ψ_0 and n_0, respectively, f_s can be written as a Taylor series about n_0 and ψ_0 as per [24], which gives

$$\gamma_{gb} = w_{gb} \{ f_{gb} - \mu_\psi (\psi_{gb} - \psi_0) - \mu_n (n_{gb} - n_0) - f_s(n_0, \psi_0) \} \quad (7)$$

where $f_s(n_0, \psi_0)$ is the free energy of a bulk solid at density n_0 and concentration ψ_0, and

$$f_{gb} = \frac{1}{L_y w_{gb}} \int_0^{L_y} \int_{x_{gb}-w_{gb}/2}^{x_{gb}+w_{gb}/2} f dx dy$$

To identify the region encompassing the grain boundary, the position along the x-axis (transverse to the grain boundary) with the maximum average free energy density is first found (x_{gb}). Properties evaluated over the entire domain, which are needed to determine the extent of segregation in the system, are then summed over all positions within $\pm$ 80 grid points of this reference position (n.b., the effective width of the system is thus taken as $w_{gb} = 161\Delta x$, because there are few differences observed when calculating the degree of segregation with $w_{gb} = 141\Delta x$, $181\Delta x$ or $301\Delta x$).

As noted by [24], the grain boundary energy is difficult to determine because f_s is difficult to determine. The system parameters were chosen to reduce the effect of residual stresses in the bulk on the calculation of the solid free energy, although this effect is observed to give a relatively uniform contribution to the energy (with the exception of when the lattice fits perfectly in the transverse direction, the bulk solid free energy varies as a random distribution with maximum spread less than 2% of its mean). Following [24], we take $w_{gb} = L_x/2$ when calculating the grain boundary energy, meaning that Eq 7 becomes to first order:

$$2\gamma_{gb} = L_x \{ f_{gb} - f_s(n_0, \psi_0) \} \quad (8)$$

For each quench temperature B_0^L and average alloy composition ψ_0, Eq. 4 was substituted for γ_{gb} in Eq. 8. The parameters f_s and A were found by fitting the resulting expression for grain boundary energy versus misorientation to our computed data. Two types of fitting were performed. The first case considered only low angles. We assumed a theoretical value for the elastic modulus E_0 analogously to Ref. [24] and obtained a best fit for f_s and A (or alternatively r_0). The elastic modulus in this case was taken from the analytic expression recently derived in Refs. [19, 23] using a one-mode approximation to the total density, i.e. by writing $n = \phi \sum_j \exp\left(\vec{G}_j \cdot \vec{x}\right)$, where $\vec{G}_j$ are the reciprocal lattice vectors of the crystal symmetry being considered (here 2D HCP). As shown in Ref. [19], Y_2 for a binary alloy is given by

$$Y_2 = 8 B^X \phi^2 \quad (9)$$
$$\phi = \frac{t + \sqrt{t^2 - 15v \left\{ \Delta B_o + (B_2^L - 4 B_0^X \eta^2) \psi_0^2 \right\}}}{15v}$$

where $\Delta B_o \equiv B_0^L - B^X$ and where ϕ is the equilibrium amplitude of the first modes of the total density n. Equation 4 is compared to the computed grain boundary energies in Fig. 2 only for bi-crystals simulated with $w = 0.088$. The coefficients E_0, A and f_s were determined as described above. In Fig. 2, the datasets are all compressed/stretched by a factor $\theta_c = r_0 \exp(0.5)/a$ to ensure that all points are fit by the normalized Eq. 4, where $E_0 = Y_2 b/(8\pi\alpha\phi^2 w_{gb})$ and $A = 1.5 - ln(2\pi)$, the latter of which is equivalent to $r_0 \approx 4.4$. The core radii, plotted in Fig. 3, can be seen to be relatively constant, though possibly decreasing for larger undercoolings $B_0^L - B_{0s}^L$ ($B_{0s}^L - B_0^X$ defines the temperature of

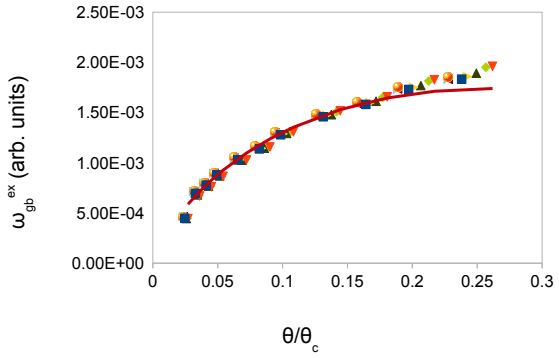

FIG. 2. Scaled grain boundary energy, $\omega_{gb} = \gamma_{gb}\Delta x\theta_c/(w_{gb}\phi^2)$, vs. normalized bicrystal crystal misorientation (in radians for the reference curve), θ/θ_c, for different concentrations and temperatures for low angles, where $\theta_c = r_0\exp(0.5)/a$ is a horizontal stretch factor. Theoretical reference Read-Shockley curve (solid); $\psi_0 = 0$, $B_0^L = 1.002$ (squares); $\psi_0 = 0$, $B_0^L = 0.962$ (inverted triangle); $\psi_0 = -0.05$, $B_0^L = 0.996$ (right triangle); $\psi_0 = -0.05$, $B_0^L = 1.006$ (circle); $\psi_0 = 0.1$, $B_0^L = 1.015$ (left triangle); $\psi_0 = 0.1$, $B_0^L = 0.995$ (star); $\psi_0 = -0.15$, $B_0^L = 1.035$ (bow tie); $\psi_0 = -0.15$, $B_0^L = 1.015$ (triangle); $\psi_0 = -0.15$, $B_0^L = 0.005$ (diamond).

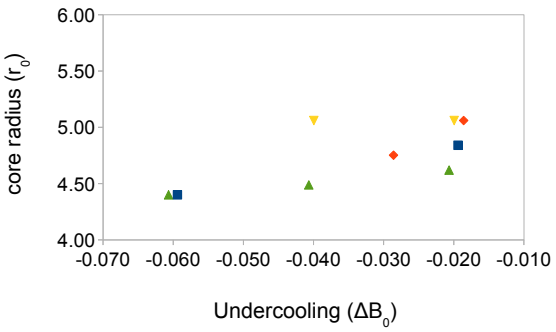

FIG. 3. Core radius versus undercooling for different concentrations calculated from low angle fit of data in Fig. 2. Square (blue) - $\psi_0 = 0$; Diamond (red) - $\psi_0 = -0.05$; Upside down triangle (yellow) - $\psi_0 = 0.1$; Triangle (green) - $\psi_0 = -0.15$

the solidus at a given concentration), consistent with the trend found in [24] for pure materials.

In the second case, all the raw data of grain boundary energy versus misorientation in Fig. 4 are scaled against a reference curve given by Eq. 4 with $E_0 = 1$ and $A = 0.362$. To match the simulated grain boundary energies to the reference curve, a vertical scaling factor $E' = E_0^m(B_0^L = 1.002, \psi_0 = 0)(\Delta x)/E_0^m(B_0^L, \psi_0)/w_{gb}$ is applied, where E_0^m are found empirically by fitting the data to Eq. 4 (discussed further below). As in Fig. 2, the

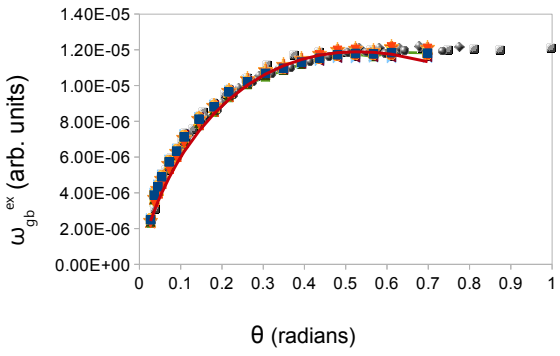

FIG. 4. Scaled grain boundary energy., $\omega_{gb} = \gamma_{gb}E_0^m(B_0^L = 1.002, \psi_0 = 0)/(w_{gb}\Delta x E_0^m(B_0^L, \psi_0))$, vs. bicrystal crystal misorientation, θ/θ_c (in radians for the reference curve) for different concentrations and temperatures. Theoretical reference Read-Shockley curve (solid). Data for $w = 0.088$: $\psi_0 = 0$, $B_0^L = 1.002$ (squares); $\psi_0 = 0$, $B_0^L = 0.962$ (inverted triangle); $\psi_0 = -0.05$, $B_0^L = 0.996$ (right triangle); $\psi_0 = -0.05$, $B_0^L = 1.006$ (circle); $\psi_0 = 0.1$, $B_0^L = 1.015$ (left triangle); $\psi_0 = 0.1$, $B_0^L = 0.995$ (star); $\psi_0 = -0.15$, $B_0^L = 1.035$ (bow tie); $\psi_0 = -0.15$, $B_0^L = 1.015$ (triangle); $\psi_0 = -0.15$, $B_0^L = 0.995$ (diamond),$\psi_0 = -0.2$, $B_0^L = 1.045$ (graduated-shading circles). Data for $w = 0.008$: $\psi_0 = -0.2$, $B_0^L = 1.065$ (graduated-shading boxes), $\psi_0 = -0.2$, $B_0^L = 1.045$ (graduated-shading diamonds),$\psi_0 = -0.2$, $B_0^L = 1.025$ (line with ties)

.

datapoints are scaled horizontally according to a stretch factor, $\theta_c = \exp(0.362 - A)$. No horizontal shift was applied to the data with $w = 0.088$ for all concentrations and temperatures (i.e., $A = 0.362$). Figure 4 also includes data from bi-crystals simulated with $w = 0.008$, which is best fit by a variety of A $(0.719, 0.467, 0.411)$, depending on undercooling ($B_0^L = 1.065, 1.045, 1.025$, respectively). In all cases shown in Fig. 4, $\eta = 0$.

The case of $w = 0.088$ and average concentration $\psi_0 = -0.15$ was also used to analyze the effect the degree of mismatch η on the thermodynamics of grain boundaries. From Fig. 5, we see that the grain boundary energy is virtually indistinguishable for the non-zero η values studied, except for some misorientations where the mismatch strains the structure a fair bit locally (most noticeable for $B_0^L = 1.035, \eta = 0.05$ at $4.13 - 8.28°$, but also noticeable for $\eta = 0.1$ at some of the higher angles), thereby increasing the free energy of the system. For $8.28°$ it was observed that for larger η that the boundary buckles, thereby relieving some of the stress. The $\eta \neq 0$ case is observed to give only a small change in total interface segregation compared to the $\eta = 0$ cases. This occurs because η does not change the amplitude of the density field much, meaning that the Read-Shockley prefactor should be approximately the same. This, in

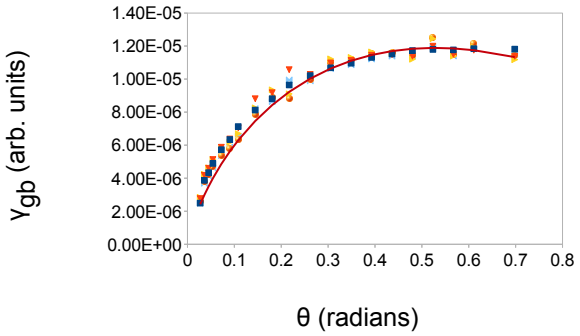

FIG. 5. Grain boundary energy at different degrees of mismatch. Blue squares, cyan ties - $\eta = 0$, green triangles, yellow triangles - $\eta = 0.05$, cyan ties, orange shaded balls - $\eta = 0.1$

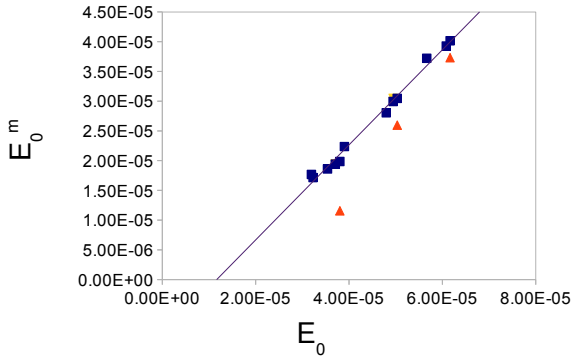

FIG. 6. Effective E_0^m fit from simulation data vs. low-angle theoretical E_0. The line of best fit for the points with $\eta = 0$, $w = 0.088$ has a slope of 0.80 ± 0.01 (squares). The points for $w = 0.008$ are triangles. Their E_0^m is approximately lower by a factors of approximately 1.4, 1.1, 1.05 for $B_0^L = 1.065, 1.045, 1.025$, which is consistent with their differences in A. The points for $\eta \neq 0$ are labeled by the upside-down triangles

turn, lead to similar grain boundary energies for the two cases, as discussed further in Section IV D).

The data of Figs. 4 and 5 was well-described by the Read Shockley relationship using the same A for all the undercoolings and concentrations studied, differing only between the alloys studied (i.e. $w = 0.088$ or $w = 0.008$). This implies that for a given alloy system, all the curves have a maximum at the same angle. For these cases, the low angle behaviour of the data should should independently obey Eq. 4 with the same theoretical expression of E_0 defined through Eq. 9. This implies that the effective, empirically-fit, E_0^m should be related to the theoretical one by a factor of around 0.65-0.85, which is the approximate ratio of $A - \ln\theta$ between the two fitting schemes for $2^\circ < \theta < 12^\circ$ (empirical method typically works because of the scatter in the data at low angles). The data of Fig. 6, which show that the theoretical and empirical values of E_0 are related via an affine transformation with slope of 0.80 ± 0.01 (for the case of $w = 0.088$), is suggestive of this conjecture. The linear fit in Fig. 6 does not pass through the origin which might suggest that this fit is inappropriate for solids with small amplitudes. This consideration is not of concern because the relation need only hold for amplitudes larger than $t/15v$, which is the smallest amplitude a solid can have in the PFC model (Eq. 9).

C. Characterizing Solute Segregation in the PFC Model

With a semi-analytical characterization for γ_{gb} in hand, we can proceed to derive an expression for the segregation at grain boundaries as a function of undercooling and alloy concentration using the Gibbs' Adsoprtion Theorem defined by Eq. 5. As mentioned above, segregation controls several important material properties, such as grain boundary melting, second phase formation, grain boundary diffusion, creep, etc.

We begin by noting that in terms of the notation used in the PFC alloy model, the expression for excess solute in Eq. 5 can be recast as

$$\begin{aligned}\left(\frac{\partial\gamma_{gb}}{\partial\mu_\psi}\right)_{T,p} &= \left(\frac{\partial\gamma_{gb}}{\partial\mu_\psi}\right)_{T,V} - V_{ex}\left(\frac{\partial p}{\partial\mu_\psi}\right)_{T,V} \\ &= \left(\frac{\partial\gamma_{gb}}{\partial\psi}\frac{\partial\psi}{\partial\mu_\psi}\right)_{T,V} - w_{gb}\frac{n_s - n_g}{1+n_s}\psi \\ &= -\Gamma_\psi^{ex} \end{aligned} \tag{10}$$

where it is understood that the formal thermodynamic variable T is to be identified by and substituted by the reduced temperature variable B_0^L of the PFC model, and w_{gb} is the width of grain boundary region. Both derivatives in Eq. 10 can be determined by making use of Eq.4 and Eq.9, and by noting that $\mu_\psi = \partial f/\partial\psi$, where $f(\psi, \phi(\psi), B_0^L)$ is the free energy density derived from the PFC model from the single mode approximation of the density n. This has been derived in Ref. [19], from which it can also be shown that $\mu_\psi = (w + 6B_2^L\phi^2 - 24\eta B_0^X\phi^2)\psi + u\psi^3$. The theoretical quantity μ_ψ differs from the simulated μ_ψ, which also implies that there is a systematic uncertainty on any calculated quantities which use this value. Using the definition of μ_ψ, we obtain,

$$\frac{\partial\psi}{\partial\mu_\psi} = \frac{1}{(w + (6B_2^L\phi - 24\eta B_0^X\phi)(\phi + 2\psi)) + 3u\psi^2 + \partial\phi/\partial\psi} \tag{11}$$

and

$$\frac{\partial \gamma_{gb}}{\partial \psi} = \frac{\partial E_0^m}{\partial \phi}\frac{\partial \phi}{\partial \psi}\,\theta\,(A - \ln(\theta)) \qquad (12)$$
$$= 2\phi \frac{-0.80(B_2^L - 4\eta^2)\psi\theta(A - \ln(\theta))}{\sqrt{t^2 - 15v(B_0^L - B^X + (B_2^L - 4\eta^2)\psi^2)}}$$

Substituting Eqs. 11 and 12 into Eq. 10 yields

$$\Gamma_{\psi}^{ex} = -w_{gb}\frac{n_s - n_g}{1 + n_s}\psi$$
$$- \frac{1.60\,\phi}{(w + 6(B_2^L - 4\eta B_0^X)\phi(\phi + 2\psi\partial\phi/\partial\psi)) + 3u\psi^2}$$
$$\times \frac{((B_2^L - 4\eta^2)\psi)\theta(A - \ln(\theta))}{\sqrt{t^2 - 15v(B_0^L - B^X + (B_2^L - 4\eta^2)\psi^2)}} \qquad (13)$$

The theoretical expression in Eq. 13 is compared directly with numerical simulations of grain boundary segregation. We follow Cahn's method [2] for determining excess solute, using the variable n and ψ. This yields an expression for the excess concentration in a grain boundary:

$$\Gamma_{\psi}^{ex} = w_{gb}\left(\psi_{gb} - \frac{(1+n)_{gb}}{(1+n)_s}\psi_s\right) \qquad (14)$$

Figure 7 compares the segregation predicted by Eq. 13 to the simulated excess measured via Eq. (14). Eq. (13) uses the effective Read-Shockley coefficients found in the previous section to cover the entire range of surface energy versus angle. The comparison is very good for some system parameters for a broad range of angles (e.g., $\psi_0 = -0.05, -0.2$) and less good, but still approximately proportional for others (e.g., $\psi_0 = -0.15, 0.1$). To estimate the extent discrepancies result from the theoretical analytic one-mode approximation, the relative difference between the analytic and simulated μ_ψ is used to determine the relative uncertainties on the analytically-determined values. Fig. 8 shows the same comparison, with Eq. 13 re-derived assuming the theoretically determined Read-Shockley parameters in the first line of Eq. 12. This comparison agrees well with the numerically determined segregation measurement only for small angle data. This is to be expected since the theoretically determined Read-Shockley parameters are only rigorously expected to hold at low angles.

D. Effect of Parameters on Grain Boundary Segregation

In this section we elucidate the effect of undercooling, alloy concentration and alloy system on segregation to grain boundaries. A typical plot of the effect of various parameters is shown in Fig. 9. Temperature (ΔB_0) has a strong effect on the degree of segregation for some

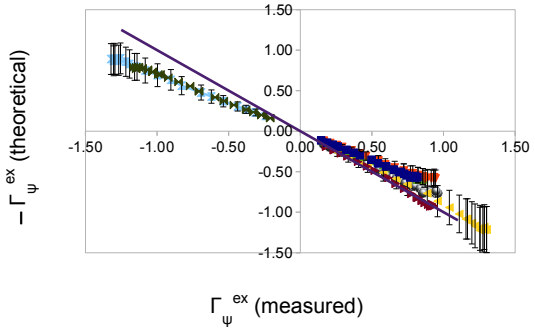

FIG. 7. Prediction of Γ_{ψ}^{ex} from Eq. 13 vs. the same quantity obtained by direct numerical simulation using Eq. 14. Uses empirically determined Read-Shockley parameters. Blue - $B_0^L = 1.015$, $\psi_0 = -0.15$; red - $B_0^L = 1.035$, $\psi_0 = -0.15$; green - $B_0^L = 0.995$, $\psi_0 = -0.15$; maroon - $B_0^L = 1.006$, $\psi_0 = -0.05$; yellow - $B_0^L = 0.996$, $\psi_0 = -0.05$; cyan - $B_0^L = 0.995$, $\psi_0 = 0.1$; dark green - $B_0^L = 1.015$, $\psi_0 = 0.1$; shaded square - $B_0^L = 1.045$, $\psi = -0.2$; shaded ball - $B_0^L = 1.015$, $\psi = -0.15$,$\eta = 0.05$. A reference line with a slope of -1 is included.

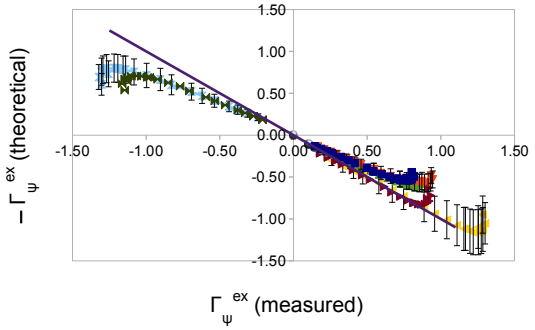

FIG. 8. Theoretical prediction of Γ_{ψ}^{ex} from Eq. 13 vs. the same quantity obtained by direct numerical simulation using Eq. 14. Uses theoretical Read-Shockley parameters. Blue - $B_0^L = 1.015$, $\psi_0 = -0.15$; red - $B_0^L = 1.035$, $\psi_0 = -0.15$; green - $B_0^L = 0.995$, $\psi_0 = -0.15$; maroon - $B_0^L = 1.006$, $\psi_0 = -0.05$; yellow - $B_0^L = 0.996$, $\psi_0 = -0.05$; cyan - $B_0^L = 0.995$, $\psi_0 = 0.1$; dark green - $B_0^L = 1.015$, $\psi_0 = 0.1$. In all cases $\eta = 0$ and $w = 0.088$ on this plot. A reference line with a slope of -1 is included.

concentrations, as seen in the difference between the red and green curve. This is due to ΔB_0 strongly affecting the density amplitude, ϕ, which in turn also affects μ_ψ. Furthermore, we see that lattice mismatch has a relatively small effect for small $|\eta|$ (< 0.1) as seen in the difference between the blue and red curves. However, the effect is larger for $\eta = 0.2$, as seen by comparing the purple and red curves. We also see that segregation is much stronger for the $w = 0.008$ alloy system (black curve) than for the $w = 0.088$ alloy system.

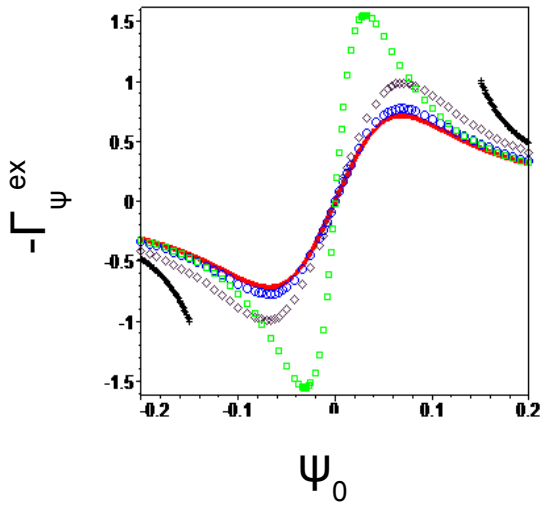

FIG. 9. Segregation at misorientation of 22.5^o for different average concentrations using Eq. 12. Red line- $B_0^L = 0.01$; Blue circle- $\eta = 0.1$, $B_0^L = 0.01$; Purple diamonds- $\eta = 0.2$, $B_0^L = 0.01$; Green square- $B_0^L = -0.01$; Black crosses- $B_0^L = 0.01$, $w = 0.008$.

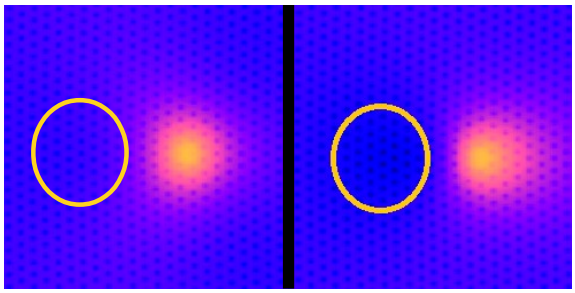

FIG. 10. Left: segregation to dislocation core with no mismatch, from part of a grain boundary at 4° misorientation for $\psi = -0.05$, $\eta = 0.0$, $B_L = 0.996$. Right: Segregation to dislocation core and Cottrell Atmosphere around a dislocation with mismatch, from part of a grain boundary at 4.14° misorientation for $\psi = -0.05$, $\eta = 0.1$, $B_L = 0.996$. Blue is small ψ and yellow is large ψ. For reference, there is a bright hollow circle to the right of the yellow/red dislocation core in each image. In the image with misfit, there is a darker blue region in the reference circle, indicating solute depletion there. The depleted solute left of the core was moved around the core, making the yellow/red region bigger than in the simulation without mismatch.

Physically, we could expect a large size mismatch between atoms, η to alter grain boundary segregation because the strains induced in the system by mis-matching local lattice constant increases the elastic free energy. To reduce free energy, solute atoms typically segregate to the grain boundary, which is typically less-ordered than the crystal. For smaller mismatch, the effect is not easily discernible. The small effect for $\eta \leq 0.1$ can be explained in terms of ϕ^2 and $\partial\mu_\psi/\partial\psi$ not changing substantially with a small change in η (these quantities depend on η^2). This effect can be visualized for low angle grain boundaries by considering the Cottrell atmosphere around a dislocation core. Assuming linear elasticity is valid and that the concentration changes do not strongly affect the stresses, the change in concentration far from a dislocation decays as [28]:

$$\Delta c = -\left\{\frac{\chi\eta Gb(1+\nu)sin(\alpha)}{\pi(1-\nu+2\chi\eta^2 E)}\right\}\frac{1}{r} \qquad (15)$$

where r is the distance from a dislocation core, E is the Young's Modulus, G is the shear modulus, where α is the angle with respect to the slip plane, ν is the Poisson ratio and $\chi = (\psi+1)(1-\psi)/\rho kT(1+(\partial\ln(a_\psi)/\partial\ln((1+\psi)/2)))$, where $a_\psi = \exp(-\mu_\psi + \mu_{\psi 0})/(\psi)$ is the activity. In our simulations, $2\chi\eta^2 E$ is small, so it is neglected from the expression. The predictions of Eq. 15 for the solute distribution field were found to approximately superimpose on the simulated solute field through the core. This simulated solute redistribution can be seen in Fig. 10 for the case $\eta = 0.1$ (right) and $\eta = 0$ (left). For larger mismatch, we expect there to be a noticeable effect on segregation as shown for $\eta = 0.2$ (purple curve) in Fig. 9. This was tested for high angles for $\psi = -0.05$, where Γ^{ex}_{ψ} increased by about 20% with a change of η from 0 to 0.2, as expected.

We found that eutectic systems exhibit stronger segregation than those with a lens-shaped (or double-lens-shaped) phase diagram. This is due to the parameter w in the binary PFC model, which is related to the difference of interspecies bond energy ϵ_{12} and self bond energies ϵ_{11}, ϵ_{22} ; that is $w \sim (2\epsilon_{12} - \epsilon_{11} - \epsilon_{22})$, where 1 and 2 represent the two kinds of atoms present. As w becomes smaller, the self-attraction becomes larger, meaning that atoms of type 1 want to be near type 1 atoms and type 2 atoms near type 2. This means that a larger degree of segregation in that this material is more energetically favourable. This is consistent with what Hondros and Seah who related solute enrichment factors (at the grain boundary) with solute solubility (which is related to $2\epsilon_{12} - \epsilon_{11} - \epsilon_{22}$) [2].

Another interesting property of the curves in Fig. 9 is that a number of the curves have a maximum and a minimum degree of segregation (concentration excess). We would expect curves in a normal material to have at least one extremum because the excess solute is zero in a pure material and non-zero value when there is a mixture; this does not contradict Hondros and Seah, who only predict a monotonic increase in surface excess Fe-P with increase P concentration because they consider small concentrations (they exclude pure P) so that they can justify using Henry's Law to determine the chemical potential

[2]. The two extrema (one minimum and one maximum) in the PFC model is partially a result of the alloy behaving mostly like a pure material for $\psi_0 = 0$, so there is one extremum between the pseudo-pure (50% composition) and each of the pure materials (0% and 100% composition). To predict at which concentration the maximum degree of segregation occurs, we could differentiate Eq. (13) with respect to ψ. This equation (and a series expansion thereof) is rather unmanageable analytically, but it is rather easily solved numerically, so this process can be adapted to other formalisms. Nevertheless, the shift of the peak with temperature observed in Fig. 9 can be understood for high angles by considering the grain boundary as being an quasi-amorphous state in equilibrium with the solid state. As temperature decreases, the amorphous state of the grain boundary becomes more metastable relative to the solid, implying that the free energy of the grain boundary increases relative to the solid. With this relative shift in free energy, a common tangent between these two "coexisting" phases steepens, making the intersection with the amorphous phase's "free energy" curve (whose minimum is closer to $\psi = 0$ than the minimum of the solid) moves closer to zero.

E. Discussion of Results

It is instructive to further consider the reasons for the weak dependence of grain boundary energy on concentration in a material where both atomic species are completely miscible in each other (i.e. the $w = 0.088$ system). As in pure materials, low angle grain boundaries in alloys are expected to have the theoretical Read-Shockley-type dependence of grain boundary energy versus misorientation. Contributions due to solute segregation, however, are expected to be minimal; this is physically the same as Turnbull's estimation of the interface energy of a heterogeneous interface, where a slight mismatch in lattice parameter leads to little contribution due to chemical energy (interface between two chemically-equivalent phases) [29]. Similarly, we found some change in grain boundary energy due to some solute segregating to the dislocation cores (as indicated by Fig. 3), but because the cores make up only a small fraction of the volume of the grain boundary, the majority of the grain boundary energy would be in the form of elastic energy associated with making a line of dislocations. Since elastic and impurity effect are both manifested via Eq. 9, other solutal effects on grain boundary energy, such as decreasing the core energy, could not be separated from the elastic effects accounted for by the parameters used in this study.

On the other hand, the grain boundary energy for high angles is expected to be roughly constant [2] and dominated by the presence of an undercooled metastable phase between the crystals [30]. This metastable phase is present throughout the entire grain boundary and so solute segregation might be expected to show a stronger effect for high angle grain boundaries than for low angle grain boundaries. Fig. 7 confirms that the degree of solute adsorption, Γ_{ψ}^{ex}, increases with angle because the larger angles have higher grain boundary energies. However, the solute segregation sometimes only decreases grain boundary energy slightly. For example, when comparing the various datasets in Fig. 4, we found that for the case of $w = 0.088$, the normalized results for $\psi_0 = 0$ datasets—which are mathematically equivalent to simulating a pure material—are essentially indistinguishable from those of a binary alloy with non-zero ψ_0.

To further demonstrate that the effect of solute segregation on the internal energy of the $w = 0.088$ system is small, we solved the linearized form of Eq. 3 in a 1D geometry. The geometry consists of two solid regions with an appropriate amplitude for the density oscillations and in between them there is a region of uniformly depressed amplitude, corresponding to an amorphous phase. The widths and amplitudes of the amorphous region are chosen to give approximately the correct amount of segregation. The change in free energy is found to be less than 10% of the total free energy, which suggests that the effect is small. If the degree of solute segregation were larger, this approach would have to be applied iteratively to both fields before inferring that the effect is small.

Some experimental and molecular dynamics studies have shown that the effect of solute segregation (modulated by the material composition) on grain boundary energy can be quite large [2, 12, 13], contrary to our grain boundary energy, which suggests (at least for the $w = 0.088$ alloys) that the change in grain boundary energy is mainly due to undercooling (which, of course, is a function of ψ at constant B_0^L), *rather than* solute segregation directly. Because the systems studied by Kirchner and Kieback [12] and Seah and Hondros [2] have limited solubility of solute in the parent phase (i.e. a eutectic alloy), we set the parameter $w = 0.008$, which simulates eutectic phase diagram, to examine if grain boundary energy changes significantly between spinodal and eutectic alloy systems. Doing so, we observed that the E_0^m for bi-crystals simulated for the $w = 0.008$ system are lower than the those of $w = 0.088$ system, as shown in Fig. 6. This suggests that segregation does, in fact, reduce grain boundary energy more significantly in eutectic alloys. Repeating calculations with the linearized form of Eq. 3 for $w = 0.088$ further reveals that the degree of segregation is higher (roughly a factor of 2). Because the degree of segregation is much larger for $w = 0.008$ than $w = 0.088$, solutal effects on the grain boundary energy depress γ_{gb} noticeably—see Fig. 6.

On the other hand, some materials, where the different atomic species have a strong affinity for each other (both species are completely miscible), include alloys with lens-shaped phase diagrams (e.g. Fe-Cr at high tem-

perature [13]) or the double lens-shaped phase diagrams (e.g. Cu-Au [1]). In both these cases, the grain boundary energy dependence on composition is observed to be very weak (if at all present), consistent with the observations reported in this work.

While we only analysed closed grain boundaries in the PFC model, Gibbs adsorption theorem, as stated in [2], suggests that it would be applicable even for wetted grain boundaries. Motivated by the 1D PF analyses of Mishin et al [6], we checked this behaviour in a 1D PF model derived from as PFC amplitude model [19], where the grain boundary is represented as a strained region. Using a T, V, μ_ψ ensemble, we can evaluate $(\partial\gamma_{gb}/\partial\mu_\psi)_T = -\Gamma_\psi = -\int dx\psi - \psi_s$ directly by varying μ_ψ (causing p to vary with it), which allowed us to verify that a premelted boundary obeys this relation in the same way a closed boundary does. This knowledge can be a powerful tool for studying premelting in alloys.

It should also be remarked that while solute segregation to grain boundaries can have significant effect on dendritic growth, where even small changes in surface energy anisotropy yield measurable changes in microstructure morphology. This was recently demonstrated by analyzing a PFC model related to the one used here in work done by Provatas et. al [22]. Another property that is expected to be more strongly affected by segregation to grain boundaries and around dislocation cores is grain boundary pre-melting behaviour, in which a system might display multiple grain boundary widths at the same state variables. These will be investigated using PFC simulations in an upcoming work.

V. CONCLUSION

The PFC alloy model has been shown in numerous works to self-consistently capture the thermodynamics and elasto-plasticity inherent in many diffusive phase transformations in metals. This work provided another test of the robustness of the PFC formalism in predicting the important physical property of solute segregation and grain boundary energy in binary alloys.

We used a phase field crystal alloy model to study solutal effects on grain boundary properties in spinodal and eutectic binary alloys. We derived a semi-empirical model of excess solute segregation to the grain boundary. This model was used to elucidate the role of undercooling, average alloy concentration, lattice misfit on the grain boundary energy on spinodal and eutectic alloys. We found that for alloys with lens-shaped phase diagrams exhibit a negligible direct contribution to the grain boundary energy, both at low and high mis-orientation angles. However, undercooling strongly impacts the energy in the PFC model through their effect on the elastic coefficients. This finding is in agreement with the findings of other groups, which found that binary materials having high solubility of one material in the other show little change in grain boundary energy with composition changes. On the other hand, we found that for a eutectic alloy system, solute segregation to the grain boundary had a stronger impact on its energy, again consistent with other works.

We also found that (small) lattice mismatches (i.e. Vegard's law parameter η) did not strongly affect segregation, though we observe that higher degrees of mismatch will have a stronger effect on segregation (as predicted by 13) and possibly because of that grain boundary energy.

There are numerous applications of the results and methodology found in this article. The phase field crystal formalism can be linked to traditional mesoscale phase field methods through various coarse graining procedures [19, 31, 32]. As a result, the grain boundary energy and segregation results inferred from this work can help guide the parameterization of mesoscale continuum theories whose forms are often—by necessity— phenomenological (e.g., [30, 33]). Similar phase field phenomenologies have been recently used to make predictions about grain boundary wetting—in particular about how the disjoining pressure changes as the system parameters change.

A simpler application of an analysis such as the one conducted here might be useful to predict when premelting should occur from the grain boundary energies and then compare it to the results observed in the binary alloy PFC model as was done for a pure material in [24]. Eventually, the PFC formalism should be applicable to more alloys with a greater number of constituent elements. We hope that this analysis is taken further by systematically analyzing the segregation properties and thermodynamic effects thereof in many materials; in conjunction with theoretical attempts, such as the one in this paper, experiments need to be done to verify their predictions and possibly uncover important, but neglected effects in the analyses.

VI. ACKNOWLEDGEMENTS

The authors acknowledge the National Science and Engineering Research Council of Canada for funding. We acknowledge Sharcnet and the Research and High-Performance Computing Support at McMaster University for computational resources. We also thank Harith Humadi, Nana Ofori-Opoku, Jeff Hoyt, Ken Elder, Michael Greenwood, Joel Berry, and Peter Stefanovic for help with code development and useful discussions.

VII. REFERENCES

[1] E. Hondros and M. P. Seah, *Physical Metallurgy*, 3rd ed., edited by R. W. Cahn and P. Haasen (North-Holland Physics Pub, Amsterdam, 1983) ISBN 0444866280, p. 855.

[2] A. P. Sutton and R. W. Balluffi, *Interfaces in Crystalline Materials* (Oxford University Press, USA, 1995) ISBN 9780199211067, p. 819.

[3] P. Lejcek and S. Hofmann, Critical Reviews in Solid State and Materials Sciences, **20**, 1 (1995), ISSN 1040-8436.

[4] J. J. Hoyt, *Phase Transformations* (McMaster Innovation Press, 2010) ISBN 978-1-926633-28-2, pp. 180–190.

[5] S. G. Mayr and D. Bedorf, Phys. Rev. B, **76**, 024111 (2007).

[6] Y. Mishin, W. Boettinger, J. Warren, and G. McFadden, Acta Materialia, **57**, 3771 (2009), ISSN 1359-6454.

[7] N. Wang, R. Spatschek, and A. Karma, Phys. Rev. E, **81**, 051601 (2010).

[8] J. Luo, Critical Reviews in Solid State and Materials Sciences, **32**, 67 (2007), ISSN 1040-8436.

[9] N. Gjostein and F. Rhines, Acta Metallurgica, **7**, 319 (1959), ISSN 0001-6160.

[10] K. Aust and B. Chalmers, American Society for Metals, **1**, 153 (1952), ISSN 0001-6160.

[11] W. T. Read and W. Shockley, Phys. Rev., **78**, 275 (1950).

[12] A. Kirchner and B. Kieback, Scripta Materialia, **64**, 406 (2011), ISSN 1359-6462.

[13] Y. Shibuta, S. Takamoto, and T. Suzuki, Computational Materials Science, **44**, 1025 (2009), ISSN 0927-0256.

[14] J. P. Hirth and J. Lothe, *Theory of Dislocations* (Krieger Publishing Company, 1992) ISBN 0894646176.

[15] S. M. Foiles, Phys. Rev. B, **49**, 14930 (1994).

[16] D. Udler and D. N. Seidman, Phys. Rev. B, **54**, R11133 (1996).

[17] K. R. Elder, N. Provatas, J. Berry, P. Stefanovic, and M. Grant, Phys. Rev. B, **75**, 064107 (2007).

[18] Y. M. Jin and A. Khachaturyan, J. Appl. Phys., **100**, 013519 (2006).

[19] K. R. Elder, Z.-F. Huang, and N. Provatas, Phys. Rev. E, **81**, 011602 (2010).

[20] K. A. Wu, A.Karma, J. J. Hoyt, and M. Asta, Phys. Rev. B., **73**, 094101 (2006).

[21] S. Majaniemi and N. Provatas, Phys. Rev. E., **79**, 011607 (2009).

[22] N. Provatas and S. Majaniemi, Phys. Rev. E, **82**, 041601 (2010).

[23] K. R. Elder and M. Grant, Physical Review E, **70**, 051605 (2004).

[24] J. Mellenthin, A. Karma, and M. Plapp, Physical Review B, **78**, 184110 (2008).

[25] J. Berry, K. R. Elder, and M. Grant, Phy. Rev. B, **77**, 224114 (2008).

[26] J. A. Warren, R. Kobayashi, A. E. Lobkovsky, and W. C. Carter, Acta Materialia, **51**, 6035 (2003).

[27] N. Provatas and K. Elder, *Phase-Field Methods in Materials Science*, 1st ed. (Wiley-VCH, Weinheim, Germany, 2919) ISBN xxxx, p. 209.

[28] F. Larche and J. Cahn, Acta Metallurgica, **33**, 331 (1985), ISSN 0001-6160.

[29] J. M. Howe, *Interfaces in Materials: Atomic Structure, Thermodynamics and Kinetics of Solid-Vapor, Solid-Liquid and Solid-Solid Interfaces*, 1st ed. (Wiley-Interscience, 1997) ISBN 0471138304.

[30] J. A. Warren, R. Kobayashi, A. E. Lobkovsky, and W. C. Carter, Acta Materialia, **51**, 6035 (2003), ISSN 1359-6454.

[31] R. Spatschek and A. Karma, Phys. Rev. B, **81**, 214201 (2010).

[32] Z.-F. Huang, K. R. Elder, and N. Provatas, Phys. Rev. E, **82**, 021605 (2010).

[33] N. Ofori-Opoku and N. Provatas, Acta Materialia, **58**, 2155 (2010), ISSN 1359-6454.